Solid Earth Discuss., 3, 615–654, 2011
www.solid-earth-discuss.net/3/615/2011/
doi:10.5194/sed-3-615-2011

Solid Earth Discussions

Using spectral analysis to detect singular events such as jerks in the geomagnetic field time series

B. Duka[1], A. De Santis[2,3], M. Mandea[4,5], A. Isac[6], and E. Qamili[2]

[1]Faculty of Natural Sciences, University of Tirana, Tirana, Albania
[2]Istituto Nazionale di Geofisica e Vulcanologia, Roma, Italy
[3]Universita' G. D'Annunzio, Chieti, Italy
[4]Institut de Physique du Globe de Paris, Université Paris Diderot, Paris, France
[5]European Center for the Arctic, Université de Versailles, Guyancourt, France
[6]Geological Institute of Romania, Bucharest, Romania

Received: 23 June 2011 – Accepted: 2 July 2011 – Published: 12 July 2011

Correspondence to: B. Duka (bejo.duka@unitir.edu.al)

Published by Copernicus Publications on behalf of the European Geosciences Union.

Abstract

In this study we have applied two spectral techniques in terms of Fourier and wavelet analysis to geomagnetic field time series and compared the results with those obtained from analogous analyses to synthetic data. Then, an algorithm has been proposed to detect the geomagnetic jerks in time series, mainly being considered by the Eastern component secular variation. Applying such analysis to time series generated from global models has allowed us to depict the most important space-time features of the geomagnetic jerks on global scale, since the beginning of XXth century. Finally, a spherical harmonic analysis of the secular acceleration power spectrum has been computed since 1960 to 2000, bringing new insights in understanding these rapid changes of the geomagnetic field and their origin.

1 Introduction

Studies of discrete time-series of different physical quantities are of a huge interest not only for their forecasting, but also for defining the nature and behavior of the underlying physical phenomena. Different methods of time-series analyses are used here to study the geomagnetic field which is, at all times, subject to temporal variations on a wide range of time scales. Most of the rapid variations originate in solar activity and solar variability (many different forms including solar flares, coronal mass ejections, solar wind sector boundaries, coronal hole streams), as well as in the Earth's environment (interactions between the solar wind and the core field). Most of the slowest variations are generated in the outer core (changes in the fluid flow), The temporal variations in the geomagnetic field cover a huge range of time-scales, from seconds to hours (external in origin), from months to decades (overlapping between external and internal changes), or from millennial to reversals (internal variations). Here, we focus on the analysis of changes in geomagnetic field, as mainly observed from magnetic observatories. This work is dedicated to analyze the short-term (likely internal) variations, observed in the geomagnetic field.

SED

3, 615–654, 2011

Courtillot et al. (1978) defined the "geomagnetic jerk" or "impulse" as a sudden change in the slope of secular variation, i.e. a discontinuity in the second time derivative (secular acceleration) of the geomagnetic field components. Considering this definition the first time-derivative (secular variation) appears as a series of straight-line segments separated by geomagnetic jerks. Nowadays, it is almost accepted they are internal in origin i.e. they are produced by fluid flows at the top of the outer core. Some attempts to explain their physical origin have been done. One of them, found in Bloxham et al. (2002), explains their origin by a combination of a steady flow and a simple time-varying, axisymmetric, equatorially symmetric, toroidal zonal flow, consistent with torsional oscillations in the Earth's core.

Usually, geomagnetic jerks are particularly visible in the Eastward component (Y), which is supposed to be the least affected by the external fields (Mandea et al., 2010). More affected by external field are the Northward component (X) and, slightly less, the vertical downward component (Z). An easy method to determine the epoch when a geomagnetic jerk occurs is to approximate secular variation time-series by straight lines and to consider the intersection point of such lines as the date of an event (Chau et al., 1981; Stewart and Whaler, 1992; De Michelis et al., 1998). During the last two decades, more powerful methods to detect geomagnetic jerks and to estimate their location and duration have been developed. For example, the wavelet analysis have been largely applied to the monthly mean series provided by different geomagnetic observatories (Alexandrescu et al., 1995, 1996; Chambodut et al., 2005), or a statistical time-series model has been used to analyze monthly means of the geomagnetic Eastward component at different observatories (Nagao et al., 2003) .

We have used three different methods of analyses to study time-series of geomagnetic field components and secular variations, with particular attention to the Y-component. All methods are essentially spectral analyses. Two of them, the Short Time Fourier Transform (STFT) and Discrete Wavelet Transform (DWT), derive directly as natural developments of Fourier Analyses, the third one being a spatial spectral analysis in spherical harmonics. The first two methods are essentially single-station

SED
3, 615–654, 2011

time series analyses, while the third one is a global spherical harmonic analysis. In this paper, we present the results of applying these methods on time-series of geomagnetic field of different observatories or time-series of synthetic data generated by different models. Thereafter, we discuss the main results, their implications in understanding the deep Earth's interior, and finally we conclude.

2 Data: observed and model-based temporal series

Before presenting the applied methods, we summarize the used data. The first kind of dataset is superior due to its length and quality: it is composed by time-series of geomagnetic field components recorded in the geomagnetic observatories on the Earth. They are chosen to be longer than 50 yr and placed as far as possible from each other. In addition, some synthetic data have been generated by means of specific functions to simulate geomagnetic jerks, in order to find the better way of the real data processing. We then generated time-series of geomagnetic field components, secular variation (SV) or secular acceleration (SA) from two geomagnetic field models described below, for a regular (uniform) grid of points over the Earth. The latter allowed us to see specific large scale behaviors of jerks over the globe. We also used the models to investigate the secular acceleration of their Gauss coefficients.

2.1 Observatory data

In this work, we have considered several observatories: Alibag (ABG), Apia (API), Chambon La Foret (CLF), Eskdalemuir (ESK), Gnangara (GNA), Hermanus (HER), Huancayo (HUA), Kakioka (KAK), Lerwick (LER), Pilar (PIL), Sitka (SIT), Vassouras (VSS), for which hourly means have been downloaded from the site SPIDR of National Geophysical Data Center (NGDC) in the format WDC. From the original hourly means of these observatories, their monthly mean values series have been also calculated.

2.1.1 A typical time-series – Niemegk observatory

A long and typical time-series the geomagnetic field has been recorded at Niemegk Observatory. The annual means series of X-, Y-, Z-components and the differences of sequential values ($\Delta X/\Delta t$, $\Delta Y/\Delta t$, $\Delta Z/\Delta t$, with $\Delta t = 1$ yr) are presented in Fig. 1. The monthly means series of X-, Y-, Z-components show the same behavior of annual means, but the differences of sequential values ($\Delta X/\Delta t$, $\Delta Y/\Delta t$, $\Delta Z/\Delta t$, with $\Delta t = 1$ month) , show that they are bearing a great amount of noise not filtered from the signal. Therefore, to remove most of the uncorrelated noise, we then applied a moving average (Olsen and Mandea, 2007) to calculate a smoothed SV (see discussion in Sect. 3.2.3). A glance at these plots underlines a few remarks. First, the same field component has the same behavior in both time-series. However, mainly for the X-component the noise level is higher in the monthly means. Second, the secular variation presents changes in its trend in the annual curves and less clear in the monthly ones.

2.1.2 Some key observatories

Amongst the considered observatories, 4 of them shown in the Table 1 have been chosen as representatives for our analyses. These observatories have been selected because they have longer and uninterrupted series of recordings, and are located at different latitudes and longitudes.

Although all the components of geomagnetic field have been studied, we will present below mainly the results for the Y-component.

2.2 Geomagnetic models

Time-series of the geomagnetic field components, their SV and SA are generated from two of most known models, i.e. CM4 (Sabaka et al., 2004) and Gufm1 models (Jackson et al., 2000). In the following, before to go into the details of the analyses, we will introduce and describe the two models.

2.2.1 CM4 model

The CM4 model (Sabaka et al., 2004) entails the parameterisation and coestimation of fields associated with the major magnetic field sources in the near-Earth regime from field measurements taken from ground-based observatories and satellite missions (POGO, Magsat , Ørsted, CHAMP). It supplies the local X-, Y-, Z-components of the ***B*** field vector from the main, lithosphere, primary and induced magnetosphere, primary and induced ionosphere, and toroidal field sources. Two evaluations of the main field are accommodated per two given spherical harmonic degree ranges for the span period 1960–2000. Using the provided FORTRAN codes of this model (http://core2.gsfc.nasa.gov/CM/CM4_A.html), we have calculated monthly time-series of Cartesian components and their SV of the main field for different places of a regular grid on the Earth's surface. These computer codes supply even time-series of the Gauss coefficients, and their first, second, third, and fourth derivatives. The capacity of this model to represent geomagnetic jerks has been already investigated (Sabaka et al., 2002; Chambodut and Mandea., 2005).

2.2.2 Gufm1 model

The gufm1 model (Jackson et al., 2000), is based on a massive compilation of historical observations of the geomagnetic field (from 1590 to 1990). For the period before 1800, more than 83 000 individual observations of magnetic declination were recorded at more than 64 000 locations; more than 8000 new observations come from the 17th century alone. Since no intensity data are available prior to 1840, the axial dipole component is linearly extrapolated back before this date. The time-dependent field model constructed from this dataset is parameterised spatially in terms of spherical harmonics and temporally in B-splines, using a total of 36 512 parameters. Using fortran codes of this model (http://jupiter.ethz.ch/~cfinlay/gufm1.html), we have generated monthly values series of X-, Y-, Z-components and their secular variations at points of a regular grid on the Earth's surface.

SED
3, 615–654, 2011

3 Methods: characteristics and application to datasets

3.1 Short Time Fourier Transform (STFT)

3.1.1 STFT – definition and representation

It is well known, that the Fourier analysis breaks down a signal into constituent harmonics of different frequencies. For regularly sampled data, Fourier analysis is performed using the discrete Fourier transform (DFT). The fast Fourier transform (FFT) is an efficient algorithm for computing the DFT of an input sequence x of length N. The output of DFT is a vector $\boldsymbol{X}$ with length N (Oppenheim and Schafer, 1989):

$$X(k) = \sum_{n=1}^{N} x(n)e^{-i2\pi(k-1)(n-1)/N}; \quad 1 \leq k \leq N \tag{1}$$

The magnitude of $|X|^2$ is called the spectrum power and its plot versus frequency is a "periodogram". Hereafter to remind the length of a vector we will put its length as index at the name. For instance, we will write x_N or $\boldsymbol{X}_N$ to indicate the signal or its DFT, both with length N. The periodogram function estimate of the PSD (Power Spectral Density) of a signal $x_N\,[n]$ is:

$$\widehat{P}_{xx}(f_k) = \frac{|X_N(f_k)|^2}{f_s N}, \tag{2}$$

where the frequencies are: $f_k = k \cdot f_s/N$, $k = 0,1,2,\ldots$, N-1 in case of a complex-valued signal; $k = 0,1,2,\ldots$, N/2-1 in case of a real-valued signal (N = even); $k = 0,1,2,\ldots$, (N-1)/2 in case of real-valued signal (N = odd); f_s is the sampling frequency. The frequency range is: [0, f_s/2] in case of a real-valued signal (N= even), [0, f_s/2) in case of a real-valued signal (N = odd) and [0, f_s) in case of a complex-valued signal.

It is obvious that considering a Fourier transform of a signal, it is impossible to indicate when particular events (such as drifts, trends, abrupt changes, etc.) appear within

SED
3, 615–654, 2011

the time-series. This deficiency can be corrected by applying the Fourier transform only to small sections of the signal at successive times, a technique called windowing the signal (Gabor, 1946) or the Short-Time Fourier Transform (STFT) (Brockwell and Davis, 2009). The STFT maps a signal into a two-dimensional function of time and frequency and can provide some information about both time and frequencies thus characterizing a particular event present in the analyzed time-series.

In order to detect particular events in long time-series of the geomagnetic field components, the secular variations (SV) or secular acceleration (SA) obtained from geomagnetic observatories, we will use the "*specgram*" function of Matlab7 software (Matlab release notes, 2004), which computes the windowed discrete-time Fourier transform of a signal using a sliding window. The spectrogram is the magnitude of this function expressed in decibel (dB). Different kinds of windows have been applied, with a different length and different overlaps, providing a sampling frequency: $f_s = 1$ (month^{-1} or yr^{-1} according to the kind of analysis). To avoid a plain spectrum in the case of geomagnetic field components, an average value of series is subtracted from each data input.

The most used windows have a Gaussian-like form (e.g. Blackman, Bohman, Chebyshev, Gaussian, Hamming, Hann, Parzen windows, to say some), and we notice that the results of spectrogram analyses almost do not depend on the form of window, although slightly depend on the window length and overlaps, and considerably depend on the length of the signal.

3.1.2 SFTF – applied to a signal generated by an analytical function

Mathematically, the jerk events are discontinuities (breakdowns) of the second derivatives of the geomagnetic field components. To test the real effectiveness of different techniques, we consider a synthetic signal which has such breakdowns in its second derivative. Then we will take advantage of the found results to apply the same processing scheme to real data.

We consider the following synthetic signal as defined in the interval [−0.5,0.5]:

$$f(t) = \begin{cases} \exp(-4t^2) & \text{for } t \in [-0.5, 0) \\ \exp(-t^2) & \text{for } t \in [0, 0.5] \end{cases}, \tag{3}$$

and sampled at every $\Delta t = 10^{-3}$. We actually rescaled the temporal abscissa as time = $500 + t \cdot 1000$, i.e. in the interval of time 0–1000. The spectrogram of the signal does not show any breakdown, but the spectrogram of the first differences of the signal values shows the breakdown close to the real one at time = 500 (Fig. 2).

Therefore, in order to detect the geomagnetic jerks by STFT, we have to study the spectrograms of the first differences of the geomagnetic field components (SV).

3.1.3 SFTF – applied to annual series of secular variation

We present here some results of SFTF analyses, firstly applied to NGK series of 116 values long (from 1890 to 2005). In case of X-, Y-, Z-component series, from the original data an average value of the series is subtracted. Thereafter, in order to get a reliable comparison of the results, the same kind of windows and same lengths of windows and overlaps are used. The spectrograms of different components show particular events at different epochs, most of them not corresponding to the known geomagnetic jerks found in literature (e.g. Mandea et al., 2010). This fact emphasizes the previous conclusion that is better to analyse the SV signals. The spectrograms of SV of X-, Y-, Z-components of NGK Observatory, calculated as the first differences of the consecutive annual means, show the evidence of particular events likely to be the geomagnetic jerks especially in the case of the Y-component (see Fig. 3).

It is obvious that spectrograms of the first differences (SV) of the field component are shifted toward the higher frequencies[1] regarding the spectrogram of the components

[1] The Fourier components of a function derivative are Fourier components of the function multiplied by the frequency. The spectrograms of the second differences (SA) (not presented here) show more clear the shift toward the higher frequencies.

themselves, and one can distinguish particular events looking at the higher frequencies band. Anyway, in case of SV of Y-component there is a clear evidence of a special event around 1969, that corresponds to the first known geomagnetic jerk noted in that epoch. One can also note some evidence of geomagnetic jerks of 1901 and 1999, but not so clear evidences of other known events.

3.1.4 STFT applied to the monthly series of secular variation

In case of monthly mean value series of the geomagnetic field components, the first differences represent very irregular and noisy signals (Fig. 1). In order to minimize this noise, mainly produced by the external field variations (ionospheric and magnetospheric variations), a moving average is applied to monthly values of SV. For example, for the Y-component, less influenced by external fields, the SV is calculated as:

$$\mathrm{SV}_y(i) = \frac{\sum_{k=0}^{n-1} Y(i+k) - \sum_{l=1}^{n} Y(i-l)}{n} \tag{4}$$

where $n = 1, 2, 3, 4 \ldots 12$, for different representatives of SV with different size of the running window. Usually, studies on geomagnetic jerks considered $n = 12$-month moving average (e.g. Mandea et al., 2000).

In the following we present the results for three different window sizes: $n = 6$, $n = 9$ and $n = 12$ for Y-component at NGK Observatory.

As it can be seen (Fig. 4) for all three chosen windows the global behavior is the same, but the larger running window is, the smoother and more de-noised the signal is. Thereafter, by using spectrograms, we can detect the geomagnetic jerks around the years: 1900, 1969 and 1990, the best case being when the moving window has a length of 12 months (Fig. 5).

Another way to get the monthly means by averaging the hourly means (slightly different from the classical one) is to compute SV according to Eq. (4) with $n = 6$. N. Olsen (IAGA 19th Scientific Assembly, Sopron-Hungary, 2009) has proposed the

SED
3, 615–654, 2011

so called "Huber average" for the hourly means, which is a robust averaging as it rejects all data that have deviation greater than a certain multiplier (Huber parameter) of the standard deviation of the data. According to his results by applying this technique and by subtraction of ionospheric (plus induced) contributions as predicted by CM4 model (Sabaka et al., 2004) and of magnetospheric (plus induced) contributions as predicted by CHAOS model (Olsen et al., 2009), the standard deviation of SV_y of NGK observatory (from 1958 to 2007) is reduced 3 times (from $\sigma = 4.7\,\mathrm{nT\,yr^{-1}}$ to $\sigma = 1.9\,\mathrm{nT\,yr^{-1}}$), while for the Chambon-la-Foret (CLF) observatory (1995–2007) is reduced from $9\,\mathrm{nT\,yr^{-1}}$ to $4\,\mathrm{nT\,yr^{-1}}$. We were not able to remove any ionospheric or magnetospheric contribution from the long series of the hourly mean data, but we have calculated the effect of using only the Huber averaging on the hourly means of Y-component of the geomagnetic field at CLF observatory (1936–2007).

In order to compare the results of the simple method of averaging and the Huber method of averaging, we have calculated the standard deviations of SV_Y of CLF observatory with different values of the Huber parameter. The results show the best cleaning of the data (the minimum of standard deviation) is achieved for the value 1.5 of Huber parameter. But the improvement on the standard deviation is almost negligible (from 4.8896 to 4.5981). This result indicates that we cannot gain too much in the cleaning of the data by using a new method of averaging. Previously results (Olsen and Mandea, 2007) which minimized standard deviation from $4.8\,\mathrm{nT\,yr^{-1}}$ to $1.9\,\mathrm{nT\,yr^{-1}}$, support the hypothesis that the most significant part of such reducing effect come from removing the ionospheric and magnetospheric contributions from the data.

3.2 Discrete Wavelet Transform (DWT)

3.2.1 DWT – definition and representation

Wavelet analysis represents a windowing technique with variable-sized regions, normally with long time intervals where we want more precise low-frequency information, and shorter time intervals where we want high-frequency information. Wavelet analysis is capable of revealing aspects of data like trends, breakdown points, discontinuities in higher derivatives, and self-similarity. It is also used to compress or de-noise a signal without appreciable degradation (e.g. Kumar and Georgiu, 1994).

Similar to Fourier analysis, wavelet analysis is the breaking up of a signal into shifted and scaled versions of the original (or *mother*) wavelet. The continuous wavelet transform (CWT) of a time function $s(t)$ is defined as the sum over all time of the signal multiplied by scaled and shifted versions of the wavelet function Ψ (Misiti et al., 2007):

$$c(a,b) = \int_{-\infty}^{\infty} s(t)\Psi(a,b,t)dt \tag{5}$$

with $a =$ scale, $b =$ position (please see also below). If a function Ψ is continuous, has null moments, decreases quickly towards 0 when t tends towards infinity, or is null outside a segment of R, it is a likely candidate to become a wavelet. Scaling a wavelet simply means stretching (or compressing) it by a scale factor a. The smaller the scale factor, the more "compressed" the wavelet. Shifting a wavelet simply means delaying (or hastening) its onset. The wavelet decomposition consists of calculating a "resemblance coefficient" between the signal and the wavelet located at position b and of scale a. The family of such coefficients $c(a,b)$ depends on two indices a and b (Kumar and Georgiu, 1994):

$$c(a,b) = \int_{R} s(t)\frac{1}{\sqrt{a}}\Psi\left(\frac{t-b}{a}\right)dt \tag{6}$$

In the Continuous Wavelets Transform (CWT), the set to which a and b belong is: $a \in R^{+} - \{0\}$, $b \in R$. In the Discrete Wavelets Transform (DWT), the scale parameter a and the location parameter b are discrete, usually based on powers of two: $a = 2^{j}$, $b = k \cdot 2^{j}$, $(j,\ k) \in Z^{2}$ (so-called dyadic scales and positions).

SED
3, 615–654, 2011

We define:

$$\psi_{j,k}(t) = \frac{1}{\sqrt{2^j}}\psi\left(\frac{t-k2^j}{2^j}\right) = 2^{-j/2}\psi\left(2^{-j}t-k\right), \tag{7}$$

identifying $\Psi_{00}(t) = \Psi(t)$. It is possible to construct a certain class of wavelets $\Psi(t)$ such that $\Psi_{j,k}(t)$ are orthonormal, i.e. the wavelets are orthogonal to their dilates and translates:

$$\int \psi_{j,k}(t)\psi_{j',k'}(t)dt = \delta_{jj'}\delta_{kk'}.$$

This implies that all such functions $\Psi_{j,k}(t)$ form a complete orthonormal basis for all functions $s(t)$ that have finite norm, i.e.: the DWT $c(j,k)$ of the time signal $s(t)$ is defined such as:

$$s(t) = \sum_{j\in Z}\sum_{k\in Z} c(j,k)\psi_{j,k}(t), \text{ where } c(j,k)=\langle s,\psi_{j,k}\rangle \equiv \int s(t)\psi_{j,k}(t)dt \tag{8}$$

Let us fix j and sum on k. A detail d_j is then the function:

$$d_j(t) = \sum_{k\in Z} c(j,k)\psi_{j,k}(t) \tag{9}$$

The signal is the sum of all the details:

$$s = \sum_{j\in Z} d_j \tag{10}$$

Let us take now a reference level called J. There are two sorts of details. Those associated with indices $j \leq J$ correspond to the scales $a = 2^j \leq 2^J$ which are the fine details. The others, which correspond to $j > J$, are the coarser details. We group these latter details into:

$$a_J = \sum_{j>J} d_j \tag{11}$$

SED
3, 615–654, 2011

which defines what is called an approximation of the signal s. We have just created the details and an approximation. The equality:

$$s = a_J + \sum_{j \leq J} d_j \tag{12}$$

signifies that the signal s is the sum of its approximation a_J and of its fine details.

In order to better identify discontinuities in the second derivative of the geomagnetic field components (monthly mean values series) registered at different observatories, we considered different kinds of wavelet shapes and level parameters among those contained in the wavelet toolbox of Matlab software (http://www.mathworks.com/help/toolbox/wavelet/). We based our choices on the known criterion:

- To detect a "rupture" in the j-th derivative, select a sufficiently regular wavelet with at least j vanishing moments.

The presence of noise makes identification of discontinuities more complicated. If the first levels of the decomposition can be used to eliminate a large part of the noise, the "rupture" is sometimes visible only at deeper levels in the decomposition.

After many attempts, the wavelets, that successfully detected the second order derivative change in the known signal (3), resulted to be the Daubechies (Daubechies, 1992) wavelet of order 4 (Db4) at level 2 of the signal decomposition:

$$s = a_2 + d_2 + d_1, \tag{13}$$

where the decomposition (Eq. 12) is stopped at $J = 2$. The results show great anomalous values of the coefficients d_1 and d_2 exactly where (time = 500) the signal (3) has the second derivative breakdown. This breakdown is better localized by the anomalous values of d_1 coefficients.

Discussion Paper | Discussion Paper | Discussion Paper | Discussion Paper |
SED
3, 615–654, 2011

3.2.2 Wavelets technique and its use for data de-noising

Synthetic data

In order to improve the results of the spectrogram function applied on the monthly series of SV, a signal de-noising is needed. We tried such de-noising by using the discrete wavelet analyses. To define empirically the best way to apply of such a technique, we generate a series of values with several spikes that have different changes of the slopes (Fig. 6). In order to have a signal more likely the secular variation registered in an observatory, we added to the original synthetic signal a colored noise generated by a Matlab function (warma) with some changes (extending and increasing of the warma-signal). These changes provide a more realistic noise (more like the SV signal) with the amplitude of the noise about 15 % of the signal itself. The composed signal and its spectrogram are shown in Fig. 6.

After applying DWT with different wavelets, the most appropriate ones in order to get the best de-noised signal are the Daubechies wavelets of order 3 and level 4. Such de-noised signal and its spectrogram are shown in Fig. 6. Based on the results regarding the synthetic signal (3), we can say that:

- The peaks or dips of the spikes, that are the abrupt changes of the slopes, are always identified by the maxima of the spectrograms. These maxima are as large as the spikes formed by the changes or slopes. The clear separations between maxima correspond to the middle of slopes and the dipper the slopes are, the narrower separations are.

- Defining an appropriate de-noising process and applying it to the composed signal (original one and noises), a spectrogram similar to that of the original signal is obtained. This new spectrogram can be easily used to identify the abrupt changes of slopes.

Considering that the added noise could overlap some frequencies of the original signal, and comparing the upper graphs in Fig. 6, it is clear that most of the singularities

SED
3, 615–654, 2011

in the curve can be identified. In this sense the operations we suggest to discriminate jerks from the rest are "conservative": what we detect is surely a jerk, even if some jerks would be missed. In the following, when applying this analysis to real data, we should take into account this fact.

5 Real data

Based on above results, we have applied this technique of de-noising the signal before doing the spectrogram, in order to identify the geomagnetic jerk events in the SV monthly means of time-series of 4 observatories described in the previous section. The obtained results are shown in the Fig. 7.

Figure 7 shows that generally the spectrograms of de-noised SV of different observatories reflect different behavior of SV in these observatories. In the low latitude observatories (for which API is considered as representative) more changes in the slope of SV can be better detected than at higher latitude observatories. These changes are smaller in amplitude and longer in time and reflect long time events such as 1950–1954 and 1996–1998 at API observatory, reflected by strong events in respective spectrograms. From the spectrogram corresponding to this observatory, it is possible to confirm some geomagnetic jerks around 1950 and 1976 at API observatory. At higher latitude observatories (for which NGK is considered as representative) the de-noising process smoothed the SV in such a way that the geomagnetic jerks that can be seen in the original signals (as around 1925 and 1978 at NGK observatory) are difficult to be detected in the respective spectrograms. Interestingly, in NGK spectrogram, geomagnetic jerks around 1901, 1969, 1990 and 1999 can be detected. Spectrograms for the middle latitude observatories (HER and KAK) indicate some different times for geomagnetic jerks. For HER observatory it makes possible to note a less marked event around 1954, a stronger one around 1986 and the strongest event of 1995. The change in the slope centered in 1972 lasts here from 1968 to 1978 and can not be considered as the signature of a geomagnetic jerk. For KAK observatory, we can identify the geomagnetic jerk of 2000, and hardly identify the jerks of 1957 and 1969. Although

SED
3, 615–654, 2011

there are intense changes in the SV of KAK observatory before 1959, these are mostly result of the registration quality during these years.

3.2.3 DWT applied to the monthly series of secular variation

To determine the second derivative breakdown of the geomagnetic field components, we apply DWT to long time series of geomagnetic field recorded at different geomagnetic observatories. The results showed evidences of different kind of events, including some of the well-known geomagnetic jerks. Better results, when jerks are easily detected, have been obtained when the DWT analyses is applied to the Y-component secular variation, calculated by the moving average window of 12 months. Before applying the DWT analyses, we have applied a de-noising procedure on the SV signal. In order to test the technique of de-noising work, we applied it to a synthetic series.

Synthetic data

The composed signal (several spikes + colored noise) represented in the Fig. 6 is de-noised by using Daubechies wavelets of order 3 and level 4 (Matlab7 wavelet Toolbox). Then, the received signal is decomposed according to Eq. (12) up to level 2 (Eq. 13) by using Daubechies wavelets of order 4 as is shown in the Fig. 8.

One can see that the maxima of the amplitude variation of d_1 and d_2 (defined in Sect. 3.2.1) coefficients correspond to the discontinuities of the first derivative of the signal.

When the signal has an abrupt and short change of the slope (about the time 835 in Fig. 8) near by another normal one, larger maxima of d_1 and d_2 coefficient variation appeared. It would render difficulties for wavelet analyses to distinguish some short local changes of SV from larger scale geomagnetic jerk events. There are also fake maxima at the edges of the time-series that must not be considered.

It can be noticed that the de-noising process improves the further analyses of SV monthly means, when aiming to detect particular events. Therefore, considering the

SED

3, 615–654, 2011

amplitude of the detailed coefficients d_1 of the signal decomposition as a measure of the second derivative breakdown of the signal, we have calculated the averaged value of such coefficients for each year of the signal duration:

$$d_1(\text{year}(k)) = \sqrt{\frac{\sum_{i=1}^{12} (d_1(\text{year}(k), \text{month}(i)))^2}{12}} \tag{14}$$

Real data

Considering again the NGK observatory, a good de-noising of the monthly value series of SV without distortions of the signal itself, are achieved by using Daubechies wavelets of order 2 level 3 or level 4, of order 3 level 4, of order 4 level 5 or level 6 decompositions (see Fig. 9). From the previous tests we can conclude that the better way to detect particular events (breakdowns of the first derivative) in such de-noised series is to use the Daubechies wavelets for the wavelet decompositions of level 2 of the same order as those used for the de-noising. Plotting the averaged values of detail coefficients d_1 (Fig. 9) of such decompositions, we see that all decompositions detect the geomagnetic jerks of 1969 and 1991, while in the higher order decomposition the particular events of 1922 and 1941 appeared. This last event, not known as a local or global geomagnetic jerk, is related to changes of the SV slope due to several spikes close to each other.

We have then applied the same way of analyses for the long monthly series of 4 geomagnetic observatories mentioned in Sect. 3.2.2. The results, not presented here, show that we have to use different order and level of wavelets for the de-noising of monthly means of SV, depending on the observatory in order to get a reasonable de-noised signal. Different kinds of decompositions of the de-noised Y-component provided by the analyzed observatories underline different particular events, some of them corresponding to well-known geomagnetic jerks. However, we can note that from some observatory data, the presence of a large number of fringe (short spikes) in the de-noised signal make very difficult the detection of geomagnetic jerks. This particularity is

SED
3, 615–654, 2011

linked not only to the difference in length of geomagnetic recordings and the data quality provided by different observatories, but also to the different behavior of Y-component SV over the Globe.

3.2.4 Global analyses

Accepting that the amplitude variation of the detail coefficient (d_1) of the decomposition of the de-noised secular variation is an indicator of the breakdown of the second derivative of the geomagnetic field components time-series, i.e. an indicator of a geomagnetic jerk, we composed the field of averaged amplitude of such a coefficient on the Earth surface. As we need long time-series of spatially uniformly distributed SV monthly values, we chose Gufm1 model to generate SV series (from 1890 to 1990) at 212 points uniformly distributed over the Earth' surface. The FORTRAN program of Gufm1 model calculates directly not only the components of the field, but even the secular variation of these components for the period of the validity of the model (from 1580 to 1990). Such a signal contains no noise as contains the SV obtained from direct measurements. For a 100-yr long (1890–1990) of monthly values series of SV_Y calculated at NGK coordinates, in the better case, we achieved the wavelet decomposition of the signal by the Daubechies wavelets of order 2 at level 2, which averaged detailed d_1 coefficients are shown in the Fig. 10. In order to detect particular events, we should consider only the d_1 coefficients that have value greater than the average (0.004) value of d_1 coefficients (these values are uncovered in the Fig. 10). Here, one can identify several events, that are undeniably known of global extension (1969, 1978), or may have a similar extension (1913, 1925), or seems to be local events (1906, 1919, 1949, 1958) (Alexandrescu et al., 1996; Le Huy et al., 1998). The largest event is a local one that lasts from 1942 to 1949 and has a central maximum at 1946.

We applied the wavelet analyses to the monthly value series of SV_Y generated by gufm1 and CM4 models at each point of the 212 points uniformly distributed over the Earth' surface. From gufm1 model we directly generate monthly values series of SV_Y for the period 1900–1990, and from CM4 model series over 1960–2002. Each time-series of all 212 points is decomposed by Db2 wavelets at level 2, saving the coefficients of decomposition. Then, we calculate the squared average value of such coefficients for every year of the period 1900–1990 for Gufm1 model and for the period 1961–2002 for the CM4 model at each of 212 points over the Earth. In such a way, we have calculated and plotted the field of d_1 coefficients at different epochs over the Earth. From such plots, we can get information about the spreading and evolution of geomagnetic field jerks. As the monthly series generated by Gufm1 model are longer than the series generated by CM4 model, the analyses results appear to be better for the Gufm1 model, therefore we present here the results for this model, only.

In Fig. 11, the fields of averaged d_1 coefficient for a selection of years from the XXth century are presented at the same scale. As we plot the deviation of d_1 coefficient value from its mean value of the whole period, the white areas correspond to the regions where the d_1 values are less than the mean value and the black areas correspond to regions where the values of the d_1 coefficient is greater than the maximum of the chosen scale. The plots of whole period can be seen in the additional movie (see Supplement).

Let us discuss, with some more details, the behavior of the d_1 coefficient derived from gufm1 model. To underline its behavior over a century an animation is available. It is indeed possible to note a relatively strong field in 1901, localized in four latitude belts mainly in the low and middle latitudes, which is followed by quiet fields from 1902 to 1904. Then two small spots of a strong field appear in 1905 over the Northern Hemisphere, gradually enlarged and expanded even in the Southern Hemisphere in 1910, 1911, 1912, to be reduced again in 1913.

Two other foci of strong field start in 1917, reaching a maximum next year and being reduced to a small spot in 1920. A quiet period follows until 1925, when a strong widespread field appears, and gradually reduces over the following years, with three remaining belts getting the strongest field on 1930–1932. From 1934 to 1940 a quiet period follows, with a few small spots at different locations, however insignificant.

From 1945 a strong field wide spreads until 1949, then two large belts of longitudes characterize the period 1950–1954. Similar shifted belts appear again in 1960, after a period of almost quiet field from 1954–1959, reaching their maxima in 1964. Another period of quiet field reaching the smallest value almost everywhere in 1967, is followed by a strong field reaching the maximum for the European area in 1969 and for a region situated in the Southern Hemisphere in 1970.

Over the time period 1972–1978 a quiet field dominates with a few small spots of strong field near the south Pole. A strong field in 1978 is observed mainly in the large west and east longitude belts. A quiet field period ends in 1982 with the appearance of two local spots of strong field: one located around African continent and the other located in the large west and east latitudes. The latest one is faded gradually in the following years, while the first one reached maximum in 1985, moving thereafter toward the South Pole and splitting in two belts of strong field in 1987. The strongest field in 1990 must be considered with caution because of the cutting edge effects.

3.3 Power Spherical Harmonic Spectra (PSHS)

The spherical harmonic analysis is a representation of the geomagnetic field potential as solution of Laplace equation, so valid from Earth's surface to ionosphere. Often, it is considered also a good representation of the potential downward the core-mantle boundary (CMB), since the magnetic and electric properties of the mantle are neglected. In order to detect any relation between the known jerk events and the time changes of the spherical harmonic of different degrees, we investigate the time variations of the Mauersberger-Lowes power spectrum terms of different degrees (Lowes, 1974, 2007) extending its definition to the secular acceleration Gauss coefficients:

$$R_n^{\mathrm{SA}} = \left(\frac{a}{r}\right)^{2n+4} (n+1) \sum_{m=0}^{n} \left[\left(\ddot{g}_n^m\right)^2 + \left(\ddot{h}_n^m\right)^2 \right] \tag{15}$$

with $a = 6371.2$ = mean radius of the Earth. We estimate the spatial power spectrum of the secular acceleration because, as a geomagnetic jerk is a step-like function in the

SED
3, 615–654, 2011

second derivative of the geomagnetic field, it can be somehow related to extremes in the power spectral density of the second derivative, R_n^{SA}.

We have used CM4 model to calculate the time-series (1960–2002) values of the secular acceleration Gauss coefficients. In the following plots, we present the time variations of R_n^{SA} for different degrees (from $n = 1$ to $n = 12$) on the Earth's surface (see Fig. 12). We do not show R_n^{SA} at the CMB because it has the same shape (the same relative minima and maxima) at both radial distances, being just the same quantity scaled by a different radial ratio $(a/r)^{2n+4}$.

In the Table 2, for each harmonics ($n = 1,..12$) we indicate by blue (or light blue) cells when the known jerk (global or local) happened at a (nearly) relative minimum of the power, by red (or orange) cells when such jerk corresponds to a (nearly) relative maximum of the power and by white cells when it does not correspond neither to a relative minimum nor maximum of the power. This extreme analysis is made because we believe that are the temporal extremes of spherical harmonic degrees that play an important role in the appearance or not of jerks.

If we look at Table 2 in terms of rows (degrees) it shows that the best coincidences of the geomagnetic jerk dates with R_n^{SA} extremes (minima or maxima) or nearly extremes (nearly minima or nearly maxima) are found for the odd degrees $n = 1$, 3 and 5 (with an exception being $n = 2$). Then, we can estimate a spreading of the geomagnetic jerks with a wavelength of: $\frac{2\pi}{n+1/2} \cdot r$ (Backus et al, 1996), i.e. from 27 000 to 7000 km on the Earth's surface. This range of spatial scales is confirmed also by the analyses of d_1 coefficient field, previously shown, where regions of the strong fields possess these spatial scales.

We do not know whether this odd degrees prevalence is just a coincidence or comes from a physical reason. We could speculate that this could come from an inherent involvement of the odd degrees in the application of the frozen-flux approximation over a hemisphere (e.g. Benton et al., 1987), but the details of why are missing at the moment and would require an extension of our work that is outside the scope the present paper.

Looking at Table 2 in terms of columns, we notice that generally the contributions of the different harmonic degrees as minima or maxima are mixed, with the only exception of 1999 jerk when all contributions are maxima or nearly maxima (apart from $N = 6$, 11 and 12 with intermediate values far from minima or maxima).

With more recent global models, which are expected to be a better representation of the present field, analogous analyses as above, could help us to better understand the different spatial contributions to jerks from all spherical harmonic degrees, and, in turn, to have a deeper look at the intrinsic sources that generate the jerks in the outer core, with some clues about the relative processes.

4 Discussions and conclusions

Over the last years, rapid changes of the geomagnetic field have been largely investigated, mainly due to the difficulty to explain the origin of such events. The recent joint analysis of ground-based and satellite data has brought some progress, mainly because of their very different distributions in space and in time. Nevertheless, such new studies need to involve a large spectra of mathematical tools to analyze the available data.

Here we show that a specific behavior can be noted mostly in different longitude belts that represent some kind of periodicity in the longitude. Particular events, such as geomagnetic jerks, having as signatures strong fields of the d_1 coefficients, are not extended over the whole globe. As shown by the available animation, starting with the 1901 event, the strong field is concentrated mostly in four longitudinal belts. The known extended 1913 jerk is represented by a strong field during 1910–1911, while the one in 1925 is represented by a strong field in four large longitudinal belts (the largest one in the center). An event around 1932 is presented by the strong field in the longitudinal belts from 1930–1932. The event of 1949 is characterized by a strong field that lasts for the longest period of time (1945–1951), covering almost half of the globe. Another particular event, presented in plots by a strong field in the South African

Discussion Paper | Discussion Paper | Discussion Paper | Discussion Paper |

SED
3, 615–654, 2011

Title Page
Abstract Introduction
Conclusions References
Tables Figures
◂ ▸
Back Close
Full Screen / Esc
Printer-friendly Version
Interactive Discussion

region over 1953-1954 has not been until now reported as a geomagnetic jerk. The well known geomagnetic jerk in 1969 is presented by a spot over Europe and an Eastern belt of strong fields during 1968–1969, followed by two large belts of strong field during 1970–1971 and the relatively strong field in the Southern Hemisphere in 1972. The 1978 geomagnetic jerk is shown by local foci of strong field over some regions of the Earth. Finally, the event in 1986 is represented by a strong field mostly over the Southern African and the south Pole region. Apart of above mentioned events, corresponding to geomagnetic jerks already noted in literature the d_1 coefficients indicate additional particular events, especially in 1917–1918, 1945–1946, 1950–1951, 1952–1954, 1963–1965, until now not reported as possible geomagnetic jerks.

Recently, Olsen and Mandea (2008) have shown that changes in the core magnetic field can be as short as a few months. These rapid secular variation fluctuations are not globally observed from satellite data. Our results obtained with analyses of both observatory and global models data are a complement of previous studies investigating the geomagnetic jerks or rapid secular variation fluctuations spatial distribution, and underline, with results covering nearly one century, that these events are not global in appearance. Also the unbalanced contributions of the spherical harmonic degrees at the different jerks is intriguing and deserves deeper attention in further studies and analyses. To conclude, all these findings are very important for continuing the present investigations on jerks to uncover more details and features of the core dynamics.

Supplementary material related to this article is available online at: http://www.solid-earth-discuss.net/3/615/2011/sed-3-615-2011-supplement.zip.

Acknowledgements. We thank N. Olsen for sending us the slides of his presentation: "Removal of External Field Contributions in Ground Observatory Data: Revised Observatory Monthly Means" of IAGA 19th Scientific Assembly, Sopron-Hungary, 2009.

SED
3, 615–654, 2011

References

Alexandrescu, M., Gilbert, D., Hulot, G., Le Mouël, J.-L., and Saracco, G.: Detection of geomagnetic jerks using wavelet analysis, J. Geophys. Res., 100(B7), 12557–12572, 1995.

Alexandrescu, M., Gilbert, D., Hulot, G., Le Mouël, J. -L., and Saracco, G.: Worldwide wavelet analysis of geomagnetic jerks, J. Geophys. Res., 101(B10), 21975–21994, 1996.

Backus, G., Parker, R., and Constable, C.: Foundation of Geomagnetism, Cambridge University Press, 103 pp., 1996.

Benton, E. R., Estes, R. H., and Langel, R. A.: Geomagnetic field modeling inconrporating constraints from frozen flux electromagnetism, Phys. Earth Planet. In., 48, 241–264, 1987.

Bloxham, G., Zatman, S., and Dumberry, M.: The origin of geomagnetic jerks, Nature, 420, 65–68, 2002.

Brockwell, P. J. and Davis, R. A.: Time Series: Theory and Methods, 2nd edn., Springer, 2009.

Chambodut, A. and Mandea, M.: Evidence for geomagnetic jerks in comprehensive models, Earth Planets Space, 57, 139–149, 2005.

Chambodut, A., Panet, I., Mandea, M., Diament, M., Holschneider, M., and James, O.: Wavelet frames: an alternative to spherical harmonic representation of potential fields, Geophys. J. Int., 163(3), 875–899, 2005.

Chau, H. D., Ducruix, J., and Le Mouël, J.-L.: Sur le caractère planétaire du saut de variation séculaire de 1969–1970, CR. Acad. Sci. Paris, B293, 157–160, 1981.

Courtillot, V., Ducruix, J., and Le Mouël, J.-L.: Sur une accélérations récente de la variation séculaire du champ magnétique terrestre, CR. Acad. Sci. Paris, D287, 1095–1098, 1978.

Daubechies, I.: Ten lectures on wavelets, CBMS-NSF Regional Conference Series in Applied Mathematics, Society for Industrial and Applied Mathematics, Philadelphia, 1992.

De Michelis, P., Cafarella, L., and Meloni, A.: Worldwide character of the 1991 geomagnetic jerk, Geophys. Res. Lett., 25, 377–380, 1998.

Gabor, D.: Theory of communications, J. Inst. Elec. Eng., 93, 429–457, 1946.

Jackson, A., Jonkers, A. R. T., and Walker, M. R.: Four centuries of geomagnetic secular variation from historical records, Philos. T. R. Soc. Lond., 358, 957–990, 2000.

Kumar, P. and Georgiu, E. F.: Wavelet Analysis in Geophysics: An Introduction, in Wavelet Analysis and its Applications, Academic Press, 1–43, 1994.

Le Huy, M., Alexandrescu, M., Hulot, G., and Le Mouël, J.-L.: On the characteristics of successive geomagnetic jerks, Earth Planets Space, 50, 723–732, 1998.

Lowes, F. J.: Spatial power spectrum of the main geomagnetic field, and extrapolation to the core, Geophys. J. Roy. Astr. Soc., 36, 717–730, 1974.

Lowes, F. J.: Spatial Geomagnetic Spectrum, in: Encyclopedia of geomagnetism and paleomagnetism, edited by: Gubbins, D. and Herrero-Bervera, E., Springer, 351–353, 2007.

MATLAB: the language of technical computing. Using MATLAB. MathWorks Inc., 2004.

Mandea, M., Bellanger, E., and Le Mouël, J.-L.: A geomagnetic jerk for the end of the 20th century?, Earth Planet. Sc. Lett., 183, 369–373, 2000.

Mandea, M., Holme, R., Pais, A., Pinheiro, K., Jackson, A., and Verbanac, G.: Geomagnetic Jerks: Rapid Core Field Variations and Core Dynamics, Space Sci. Rev., 155, 147–175, 2010.

Misiti, M., Misiti, Y., Oppenheim, G., and Poggi, J. M.: Wavelets and Their Applications, Hermes Lavoisier, ISTE Publishing Knowledge, 2007.

Nagao, H., Iyemori, T., Higuchi, T., and Araki, T.: Lower mantle conductivity anomalies estimated from geomagnetic jerks, J. Geophys. Res., 108(B5), 2254, doi:10.1029/2002JB001786, 2003.

Olsen, N. and Mandea, M.: Investigation of a secular variation impulse using satellite data: The 2003 geomagnetic jerk, Earth Planet. Sc. Lett., 255, 94–105, 2007.

Olsen, N. and Mandea, M.: Rapidly changing flows in the Earth's core, Nat. Geosci., 1, 390–394, 2008.

Olsen, N., Mandea, M., Sabaka, T. J., and Tøffner-Clausen, L.: CHAOS-2: A Geomagnetic Field Model Derived from one Decade of Continuous Satellite Data, Geophys. J. Int., 179, 1477–1487, 2009.

Oppenheim, A. V. and Schafer, R. W.: Discrete-Time Signal Processing, Prentice Hall, Englewood Cliffs, NJ, 1989.

Sabaka, T. J., Olsen, N., and Langel, R. A.: A comprehensive model of the quiet-time, near-Earth magnetic field: Phase 3, Geophys. J. Int., 151, 32–68, 2002.

Sabaka, T. J., Olsen, N., and Purucker, M. E.: Extending comprehensive models of the Earth's magnetic field with Ørsted and CHAMP data, Geophys. J. Int., 159, 521–547, 2004.

Stewart, D. N. and Whaler, K. A.: Geomagnetic disturbance fields: an analysis of observatory monthly means, Geophys. J. Int., 108, 215–223, 1992.

SED

3, 615–654, 2011

Using spectral analysis to detect singular events

B. Duka et al.

Table 1. The geomagnetic observatories that have been chosen as representatives for analyses.

IAGA code	Latitude	Longitude	Altitude (m)
API	$-13°48'$	$188°13.2'$	4
HER	$-34°25.2'$	$19°13.8'$	26
KAK	$36°13.8'$	$140°11.4'$	36
NGK	$52°4.2'$	$12°40.8'$	78

SED
3, 615–654, 2011

Table 2. Jerk years correspondences with extremes of R_n^{SA} terms.

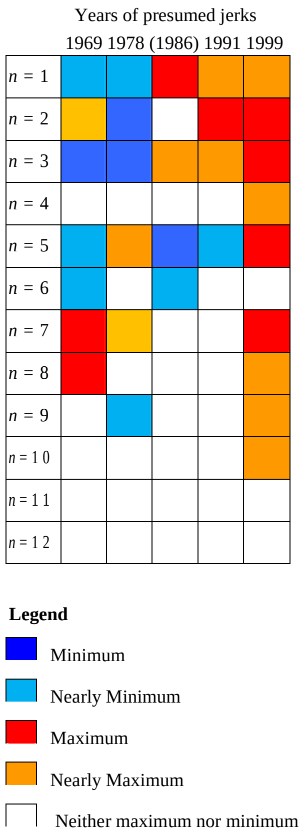

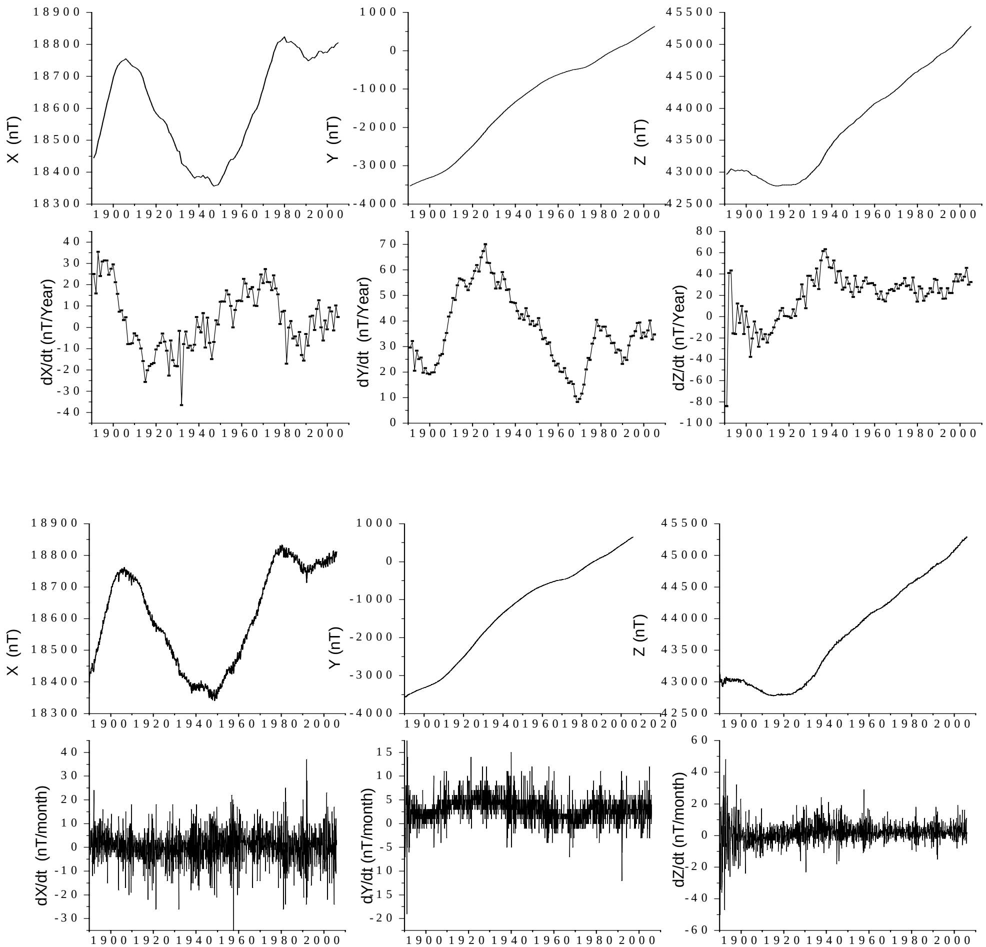

Fig. 1. Annual (up) and monthly (down) mean series of X-, Y-, Z-components and their numerical derivatives (differences of the sequential values).

SED
3, 615–654, 2011

Using spectral analysis to detect singular events

B. Duka et al.

Title Page
Abstract Introduction
Conclusions References
Tables Figures
◀ ▶
Back Close
Full Screen / Esc
Printer-friendly Version
Interactive Discussion

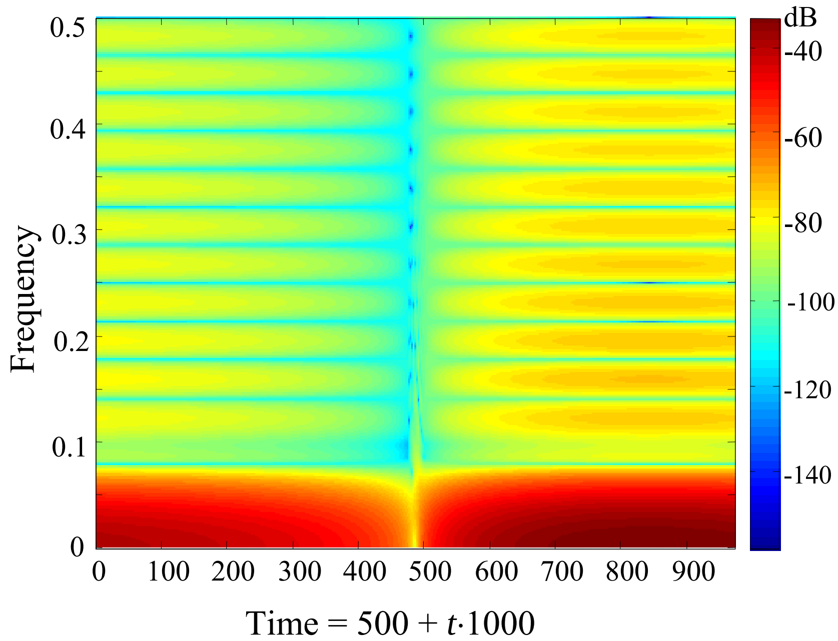

Fig. 2. The spectrogram of the first difference series of the signal (3) sampled at every $\Delta t = 10^{-3}$ with the temporal abscissa rescaled as time $= 500 + t \cdot 1000$.

SED
3, 615–654, 2011

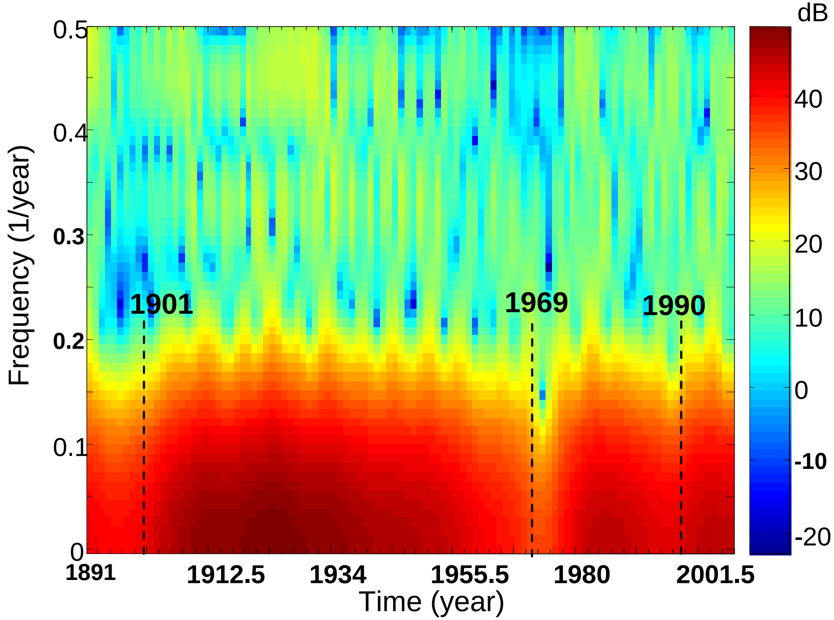

Fig. 3. Spectrogram of SV of annual mean values of Y-component recorded at NGK Observatory (1891–2005).

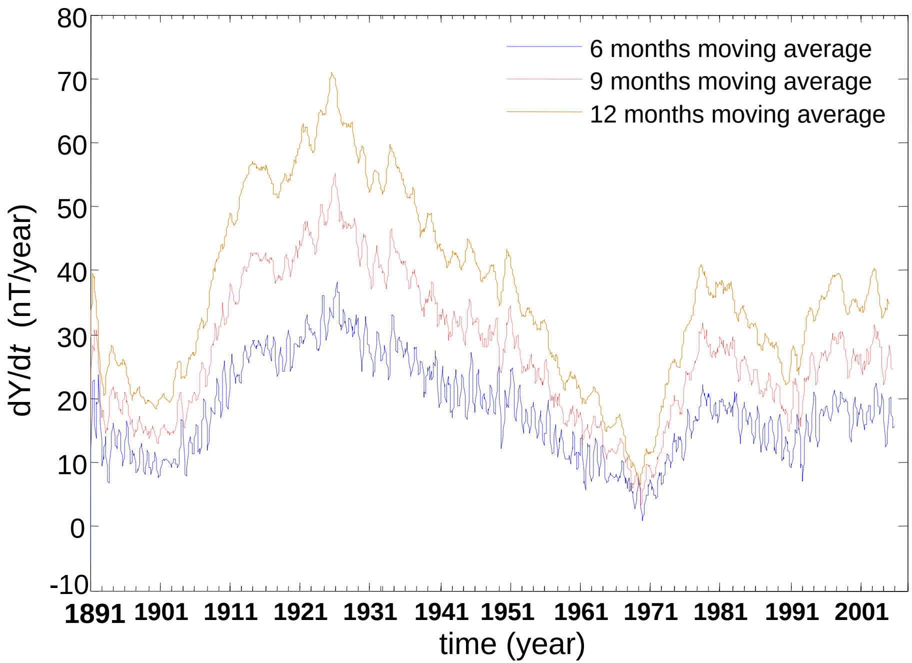

Fig. 4. Monthly values series of SV of Y-component (calculated by different moving averages) at NGK Observatory (1891–2005).

SED

3, 615–654, 2011

Using spectral analysis to detect singular events

B. Duka et al.

Title Page
Abstract | Introduction
Conclusions | References
Tables | Figures
◀| |▶
◀ ▶
Back | Close
Full Screen / Esc
Printer-friendly Version
Interactive Discussion

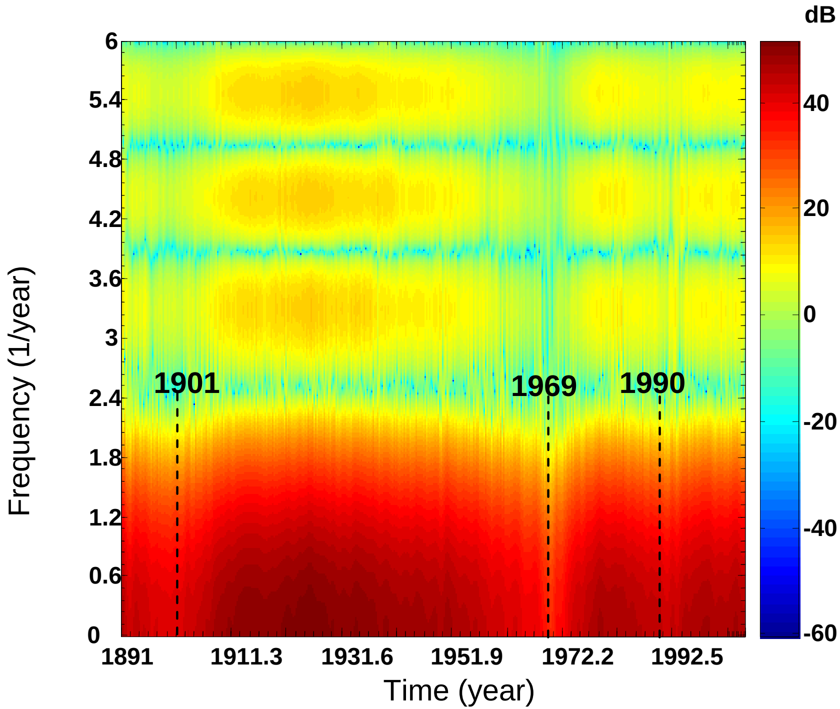

Fig. 5. Spectrogram of monthly values series of SV of Y-component (12 months moving average) at NGK Observatory (1891–2005).

SED
3, 615–654, 2011

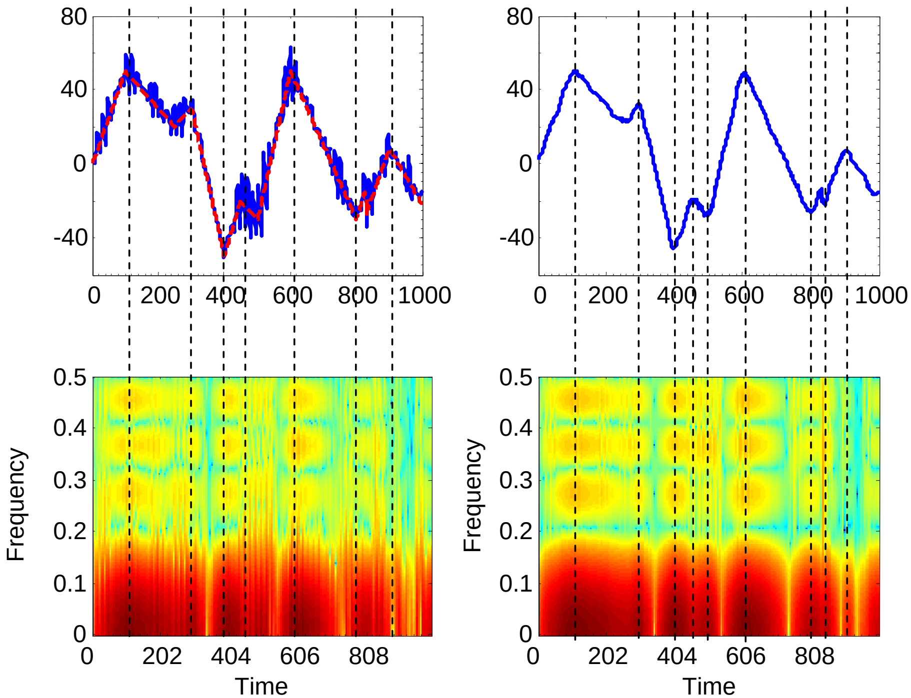

Fig. 6. Synthetic signal representing a SV-like signal (left top) composed by different spikes and a colored noise and the corresponding spectrogram (left bottom). The de-noised signal (right top) and its corresponding spectrogram (right bottom).

SED
3, 615–654, 2011

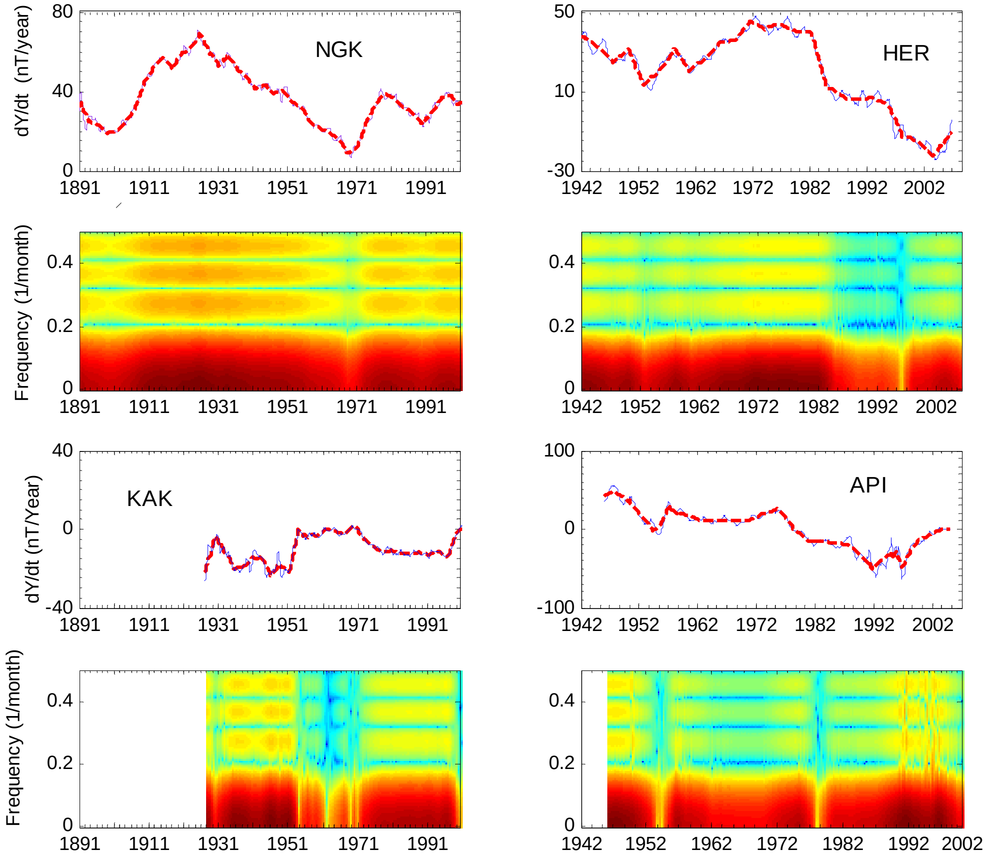

Fig. 7. The de-noised signals of secular variations ($SV_y = dY/dt$) of NGK, KAK, API and HER observatories and their respective spectrograms.

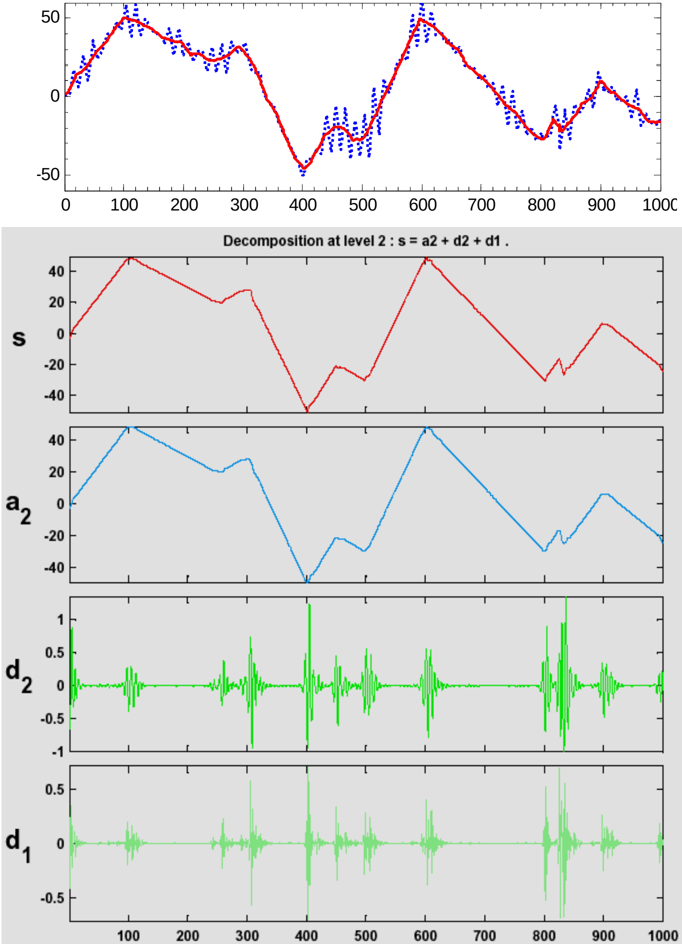

Fig. 8. The synthetic composed signal (spikes + colored noise) and its de-noised signal (up); the decomposition of the de-noised signal up to level 2 (down).

SED
3, 615–654, 2011

Using spectral analysis to detect singular events

B. Duka et al.

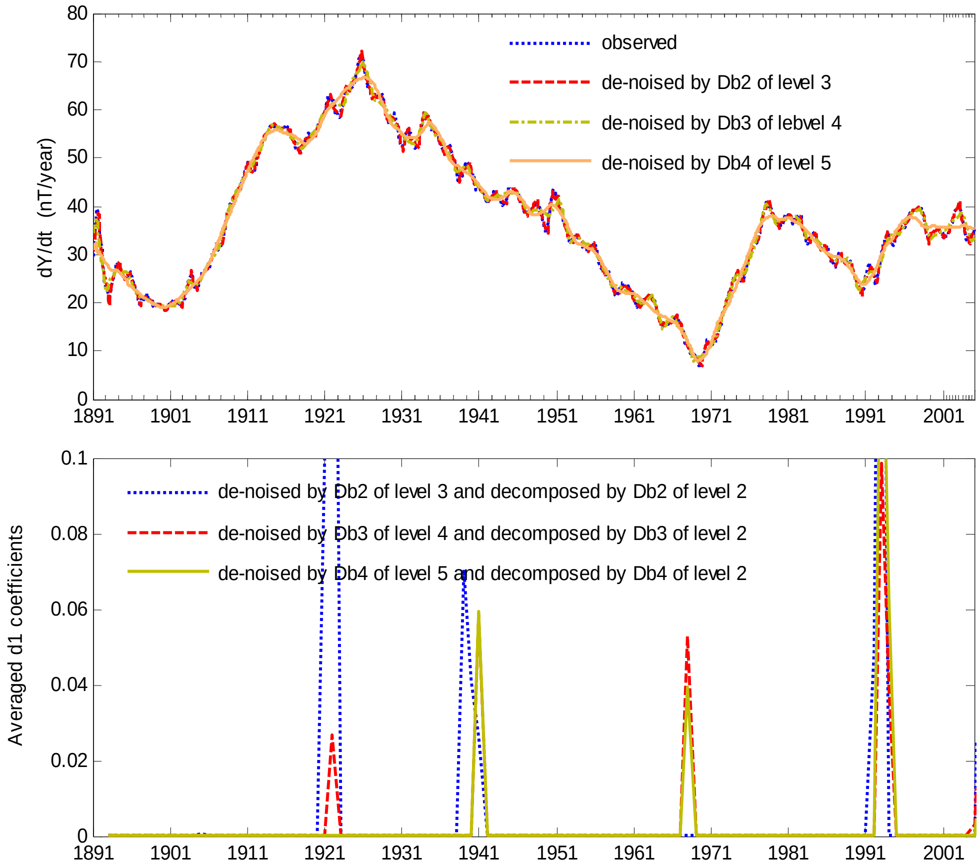

Fig. 9. De-noised SV_Y signal of NGK (up) and the respective values of averaged d_1 coefficients (down).

SED
3, 615–654, 2011

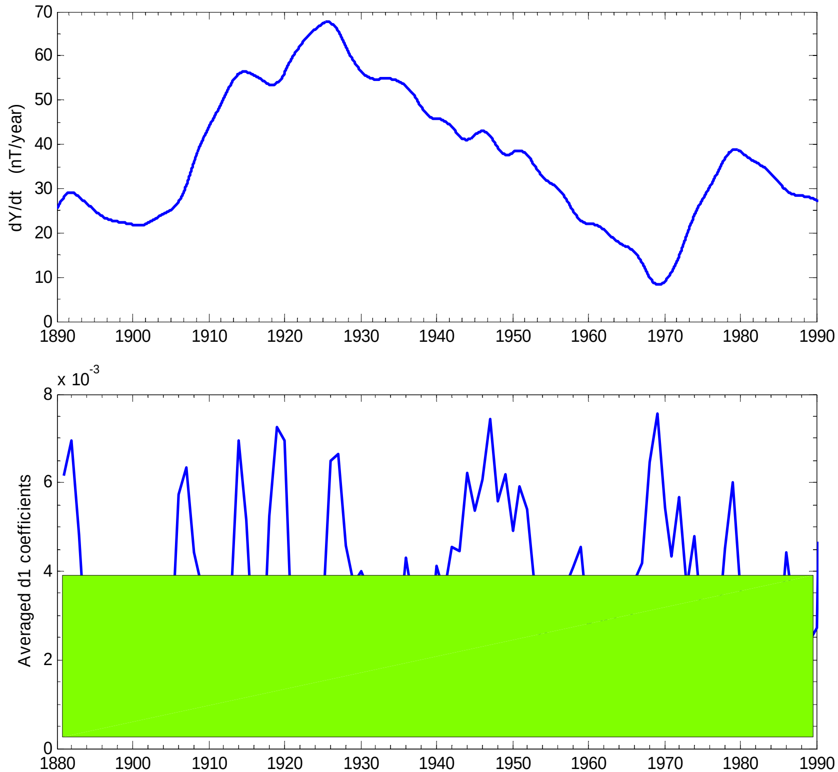

Fig. 10. Monthly value series of SV of Y-component generated by gufm1 model at NGK Observatory for the period 1890–1990 (up) and averaged d_1 coefficients of the series decomposition by Db2 wavelets of level 2. The d_1 coefficients below their mean value are hidden.

SED
3, 615–654, 2011

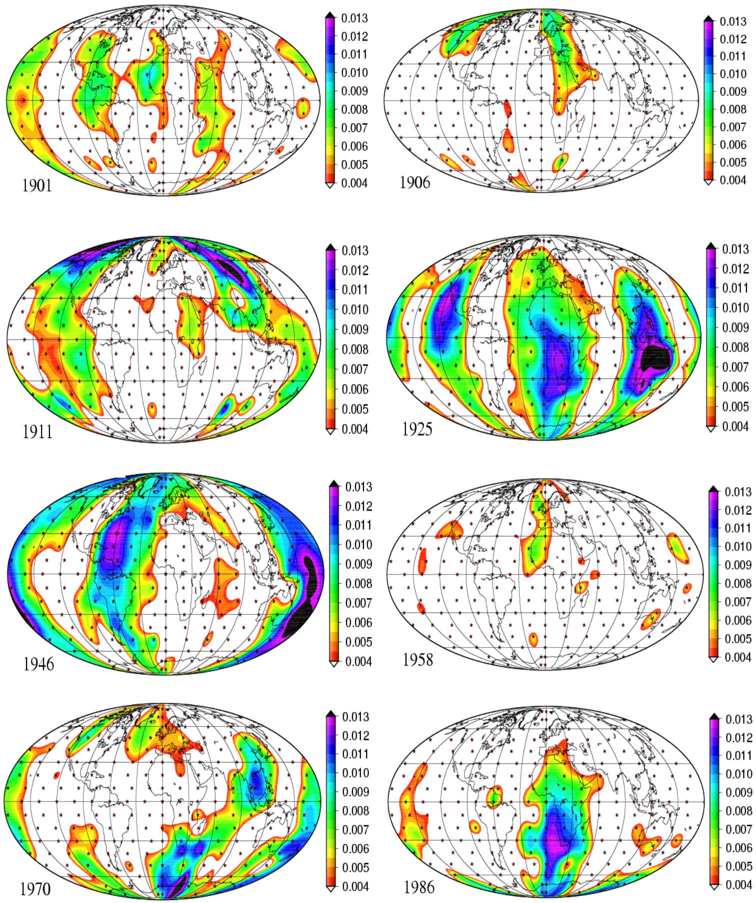

Fig. 11. An example of the d_1 coefficient field behavior, for the epochs: 1901, 1906, 1911, 1925, 1946, 1958, 1970, 1986, which are a selection from the complete movie in the Supplement.

SED
3, 615–654, 2011

Using spectral analysis to detect singular events

B. Duka et al.

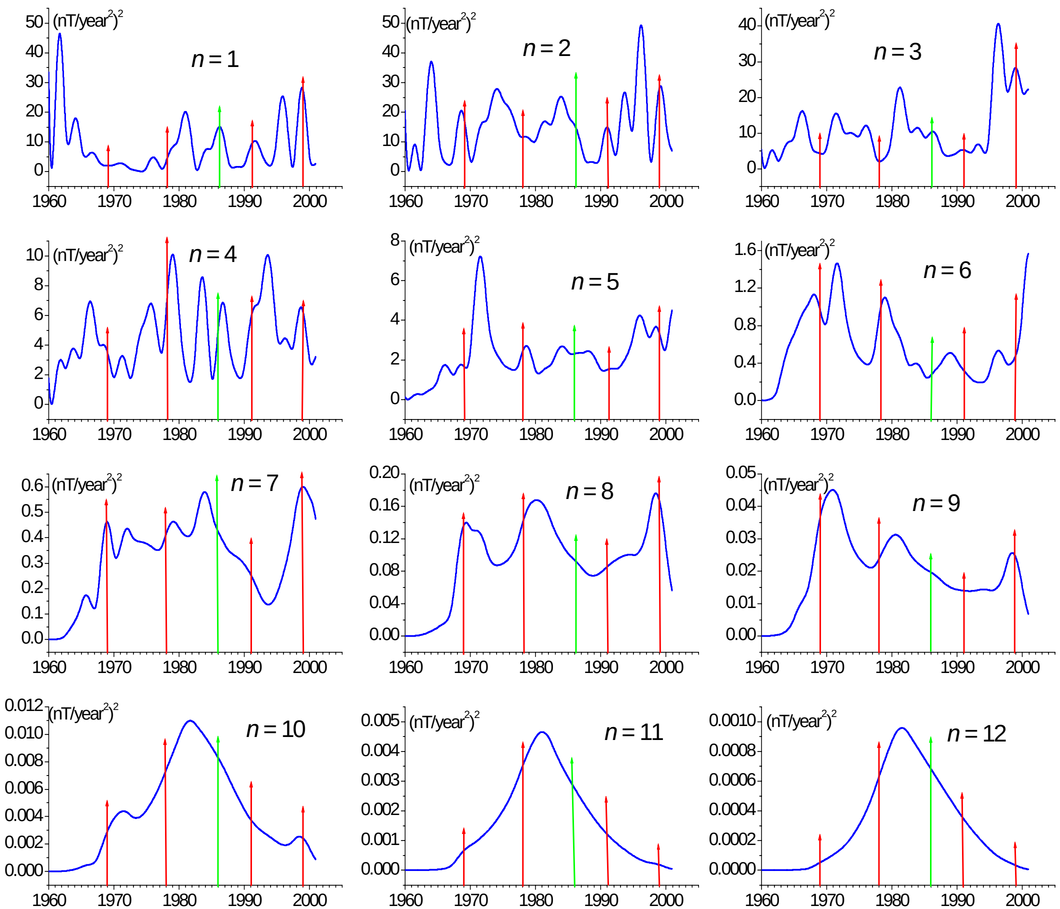

Fig. 12. Time variations of the spherical power spectra terms (R_n^{SA}) at the Earth surface.

SED
3, 615–654, 2011